

MIT Open Access Articles

*Compressibility of an ultracold Fermi
gas with repulsive interactions*

The MIT Faculty has made this article openly available. **Please share**
how this access benefits you. Your story matters.

Citation: Lee, Ye-Ryoung et al. "Compressibility of an Ultracold Fermi Gas with Repulsive Interactions." *Physical Review A* 85.6 (2012): 063615. © 2012 American Physical Society.

As Published: <http://dx.doi.org/10.1103/PhysRevA.85.063615>

Publisher: American Physical Society

Persistent URL: <http://hdl.handle.net/1721.1/72453>

Version: Final published version: final published article, as it appeared in a journal, conference proceedings, or other formally published context

Terms of Use: Article is made available in accordance with the publisher's policy and may be subject to US copyright law. Please refer to the publisher's site for terms of use.



Compressibility of an ultracold Fermi gas with repulsive interactions

Ye-Ryoung Lee,¹ Myoung-Sun Heo,¹ Jae-Hoon Choi,¹ Tout T. Wang,^{1,2} Caleb A. Christensen,¹ Timur M. Rvachov,¹ and Wolfgang Ketterle¹

¹*MIT-Harvard Center for Ultracold Atoms, Research Laboratory of Electronics, Department of Physics, Massachusetts Institute of Technology, Cambridge, Massachusetts 02139, USA*

²*MIT-Harvard Center for Ultracold Atoms, Department of Physics, Harvard University, Cambridge, Massachusetts 02138, USA*

(Received 18 April 2012; published 21 June 2012)

Fermi gases with repulsive interactions are characterized by measuring their compressibility as a function of interaction strength. The compressibility is obtained from in-trap density distributions monitored by phase-contrast imaging. For interaction parameters $k_F a > 0.25$, fast decay of the gas prevents the observation of equilibrium profiles. For smaller interaction parameters, the results are adequately described by first-order perturbation theory. We have developed a phase-contrast imaging method that compensates for dispersive distortions of the images.

DOI: [10.1103/PhysRevA.85.063615](https://doi.org/10.1103/PhysRevA.85.063615)

PACS number(s): 03.75.Ss, 67.85.Lm, 05.30.Fk

I. INTRODUCTION

Experiments with ultracold atoms explore many-body physics with strong interactions. They have demonstrated long-predicted phenomena like the BEC-BCS crossover [1] and Lee-Huang-Yang corrections to the energy of degenerate gases [2–4]. Experiments have also explored novel quantum phases like fermions with unitarity-limited interactions [1,5], population-imbalanced Fermi gases [6,7], and Hubbard models in optical lattices [8,9]. More recently, they have been used to provide precision tests of many-body theories [5]. Usually, interactions in ultracold gases are fully described by the scattering length, which is a zero-range approximation greatly simplifying the theoretical description. This approximation is valid since the diluteness of the atomic gases implies a particle separation much larger than the short range of the van der Waals interactions. This almost exact characterization of the interactions by a single parameter, the tunability of interaction strength, and precise experimental control over cold-atom systems have made them an ideal test bed for many-body quantum calculations.

A new level of quantitative comparison between theory and experiment was recently reached by careful measurements of density profiles from which the equation of state could be determined. These techniques were first proposed by Chevy [10] and Bulgac and Forbes [11] and implemented by Shin [12]. Further improvements [4,5,13–16] resulted in impressive accuracy without adjustable parameters. These results hinge on accurate measurements of the equilibrium atomic density distribution. Since all cold-atom systems are in a metastable phase, this requires a favorable ratio of lifetime to equilibration time.

Long lifetimes and strong interactions were realized in Fermi gases with strong attractive interactions since the decay to lower-lying molecular states is suppressed by the Pauli exclusion principle [17]. This is different for repulsive interactions which are realized on the so-called upper branch of a Feshbach resonance, where decay is always possible into the so-called lower branch, which consists of weakly bound molecular states with binding energy \hbar^2/ma^2 where a is the scattering length.

For bosons, the first beyond-mean-field correction, the so-called Lee-Huang-Yang term, could be observed, but corrections were necessary to account for the nonequilibrium

profile, since the time to sweep to strong interactions was not long compared to equilibration times and inverse loss rates [3]. Here we study fermions with repulsive interactions. They have been the focus of much recent work due to the prediction of a phase transition to a ferromagnetic state for sufficiently strong interactions [18,19]. Recent experimental [20,21] and theoretical studies [22] addressed the competition with strong decay to the lower molecular branch.

As expected we find only a limited window for metastability where we can observe equilibrated clouds and characterize the repulsive interactions by obtaining the compressibility from observed profiles. We observe the linear term in $k_F a$ corresponding to mean-field energy in density profiles. k_F is the Fermi wave vector. In contrast to a Bose-Einstein condensate, here the mean-field energy is smaller than the kinetic energy and also competes with the thermal energy, and is therefore much more difficult to observe. The signal-to-noise ratio (and some heating) prevented us from discerning the second-order interaction term which is the Lee-Huang-Yang correction for fermions.

Our work employs phase-contrast imaging using two different laser detunings to identify and correct for dispersive distortions of the cloud. All studies mentioned above, with one exception [12], were conducted using resonant absorption where dispersion (an index of refraction different from 1) is absent. However, this severely limits the cloud size and number of atoms to small optical densities. Phase-contrast imaging has many advantages. It can be applied to clouds with much larger optical densities by adjusting the detuning. Due to coherent forward scattering, the heating effect per detected signal photon is reduced by potentially a large number (which is equal to the resonant optical density divided by 4 [23]). This can, e.g., be used for repeated nondestructive imaging. However, for precision studies of density profiles, small dispersive distortions of the density profile cannot be neglected. Previous work including Ref. [12] was not sensitive to this effect. We have developed an experimental technique to correct for dispersion.

II. EXPERIMENTAL SETUP

A spin-polarized Fermi gas of ${}^6\text{Li}$ in the $|F = 3/2; m_F = 3/2\rangle$ state is produced by sympathetic

cooling with bosonic ^{23}Na atoms in a magnetic trap as described in [24]. The ^6Li atoms are then loaded into a single-beam optical dipole trap and transferred into the lowest hyperfine state $|F = 1/2; m_F = 1/2\rangle$ by a Landau-Zener radio-frequency (rf) sweep. Additional axial confinement is provided by magnetic field curvature. An equal mixture of $|1\rangle$ and $|2\rangle$ spin states (corresponding to the $|F = 1/2; m_F = 1/2\rangle$ and $|F = 1/2; m_F = -1/2\rangle$ states at low magnetic field) is prepared by a rf sweep at 300 G, followed by 500 ms wait time for decoherence and evaporative cooling in the optical trap. The Feshbach resonance at 834 G [1] is used to tune the repulsive interactions between $|1\rangle$ and $|2\rangle$. We increase the magnetic field in 200 ms to 528 G, where the scattering length is zero and our Fermi gas is noninteracting. The final trap has a depth of $4.1 \mu\text{K}$ and frequencies of $\omega_x = \omega_y = 390 \text{ Hz}$ and $\omega_z = 34.7 \text{ Hz}$. The number of atoms per spin state is 8×10^5 , which corresponds to a Fermi temperature T_F of $1.4 \mu\text{K}$. The temperature of the atoms is $0.3T_F$ at this point. For loss rate measurements, the magnetic field is quickly ramped to the target field. For compressibility measurements, the field is ramped up over 50 ms and held for 30 ms to ensure thermal equilibrium before imaging. The molecular fraction in the density profile is determined by dissociating molecules with a magnetic field jump to 20 G above the Feshbach resonance, and comparing with the atom number after jumping to 528 G where the cross section for imaging molecules vanishes (see Ref. [25]).

III. LOSS RATE

To obtain thermodynamic parameters from atomic density profiles requires equilibration. One time scale for equilibration is set by the longest trap period, which is 30 ms for the axial direction. The authors of Ref. [3] studied the distortions of profiles of bosonic ^7Li due to nonadiabatic ramping of the scattering length. The authors found that ramping times longer than $\approx 6\pi/\omega$ (which is 90 ms for our parameters) led to only small deviations from equilibrium profiles. Here, ω is the smallest of the trapping frequencies, which sets the time scale for equilibration. Assuming that losses sharply increase during the last 5 ms of the ramp towards stronger interactions and limiting tolerable losses to 10% leads to an estimate of a maximum tolerable loss rate of about 0.02/ms. The fastest relaxation time for excitations created during a nonadiabatic ramp is $1/\omega$ (the damping time for a harmonic oscillator at critical damping). Allowing $\sim 10\%$ loss during this time leads to an identical estimate for the tolerable loss rate of $\sim 0.02/\text{ms}$.

We measured loss rate as a function of interaction strength $k_F^0 a$. Note that k_F^0 is the Fermi wave vector of the zero-temperature noninteracting gas calculated at the trap center using total atom number. The real k_F is somewhat smaller because repulsive interactions and nonzero temperature lower the density.

First, in Fig. 1(a) we measured the number of atoms right before and after the fastest possible ramp (limited to 7 ms by eddy currents) to the target magnetic field. During the ramp to the target magnetic field of $k_F^0 a \approx 0.8$, $\sim 35\%$ of the sample is lost. Measuring the loss rate at higher $k_F^0 a$ is difficult because most of the sample is lost even before reaching the target fields. The loss rate was determined by monitoring the drop

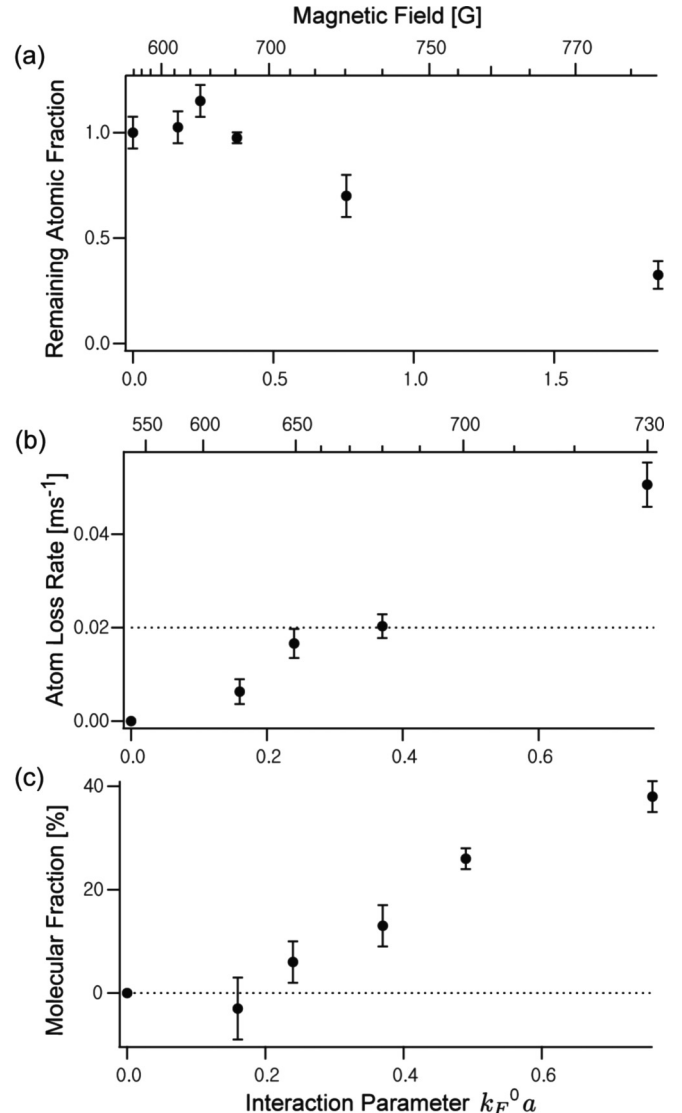


FIG. 1. Characterizing atomic loss for increasing repulsive interactions. (a) Remaining fraction of atom number immediately after the fastest possible ramp to the target field. (b) Atom loss rates at the target fields. Dashed line shows the estimated maximum tolerable loss rate of 0.02/ms. (c) Molecular fraction after the 50 ms ramp and 30 ms wait time, corresponding to when we measure equilibrium atomic density profiles.

in the number of atoms immediately after the field ramp. The results in Fig. 1(b) show that the measured loss rate reaches the maximum tolerable value of 0.02/ms at $k_F^0 a \approx 0.35$, limiting our measurements of equilibrium density profiles to smaller values of $k_F^0 a$. Furthermore, at the same values of $k_F^0 a$, the molecular fraction when we measure equilibrium density profiles exceeded 10% [see Fig. 1(c)]. As we discuss in Sec. IV the presence of a molecular component affects the compressibility measurement.

IV. COMPRESSIBILITY MEASUREMENT

A system is characterized by its equation of state. The equation of state can be expressed in different forms involving various thermodynamic variables including density, energy,

pressure, temperature, and entropy. For cold-atom experiments, density, chemical potential (through the trapping potential), and temperature are directly accessible to measurement. In the weakly interacting regime, the interaction manifests itself as a perturbative term in the equation of state. Here we measure this perturbative interaction effect by measuring the derivative of density with chemical potential, the isothermal compressibility of the gas. We prepare the system at the lowest temperature, but due to heating of the cloud by molecule formation, we have to apply a correction for the measured finite temperature.

Using the experimental procedure discussed above, we prepared equilibrated clouds at various magnetic fields and measured line-of-sight integrated profiles of column density using *in situ* phase-contrast imaging [26]. The signal-to-noise ratio was improved by averaging the column density along equipotential lines (which are ellipses for the anisotropic harmonic oscillator potential). The averaging region was restricted to an axial sector of $\pm 60^\circ$ to avoid corrections due to transverse anharmonicities [27]. Three-dimensional density profiles $n(r)$ were reconstructed by applying the inverse Abel transformation to the column densities $\tilde{n}(r)$ [26].

The isothermal compressibility is obtained from a spatial derivative of $n(r)$, since in the local density approximation, the local chemical potential is $\mu = \mu_0 - m\omega^2 x^2/2$, where μ_0 is the global chemical potential and ω the trap frequency. The compressibility is defined as

$$\kappa = \frac{1}{n^2} \frac{\partial n}{\partial \mu}. \quad (1)$$

We normalize the compressibility κ by the compressibility of an ideal gas at the given density and zero temperature $\kappa_0 = \frac{n^{1/3}}{n^2} \frac{3m}{\hbar^2 (6\pi^2)^{2/3}}$, and obtain the normalized compressibility

$$\tilde{\kappa} = \frac{\kappa}{\kappa_0} = \frac{\hbar^2 (6\pi^2)^{2/3}}{2m} \frac{\partial n^{2/3}}{\partial \mu}. \quad (2)$$

Here n is density, and m is the atomic mass. The normalized compressibility is obtained as the slope in a plot of $n^{2/3}$ vs μ (Fig. 2). This plot is in essence the observed density profile plotted with the central region to the left and the spatial wings to the right. Experimentally, we find the slope to be constant over an extended range of the density profile. Compressibilities were determined from fits to the slope in the region of 90% to 50% of the peak density. The region near the center of the cloud was excluded since the center is singular for the inverse Abel transformation, leading to excessive noise. These compressibilities should be regarded as average values over the density range used in the fit. The uncertainty of fitting the slope to a single profile was 4.5%. By averaging the profiles obtained from 20 images, the uncertainty was improved to 1.3%.

The normalized compressibility is a function of T/T_F and $k_F a$. At finite temperature and scattering length a , T/T_F and $k_F a$ change across a single density profile because T_F and k_F depend on the local density. However, this density dependence is small near the center of the cloud. Simulated density profiles showed that the average compressibility determined in the way described above agrees to within 0.6% with the compressibility

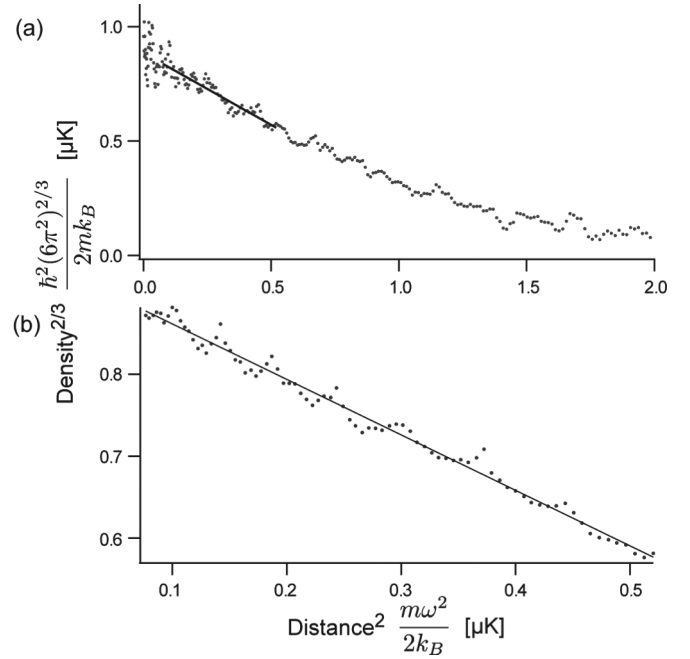


FIG. 2. Determination of the compressibility of repulsively interacting Fermi gases. The compressibility is the slope of a graph showing the density to the power $2/3$ versus the square of the distance from the center. (a) Single-shot density profile. (b) Closeup of the region used for determining the compressibility for a plot showing the average of 20 density profiles.

at T/T_F and $k_F a$ at the density in the center of the selected range.

Compressibility decreases for stronger repulsion, but also for higher temperature. To identify the effect of repulsive interaction requires a careful consideration of finite temperature effects. First, the temperature of the cloud had to be accurately determined. This can be done without any special assumptions by fitting the wings of the cloud using a virial expansion [28], by thermometry with another cotrapped atom [14], or for population imbalanced clouds by fitting the wings of the majority component which is an ideal Fermi gas [29]. Here we chose to determine temperature using a virial expansion,

$$p \frac{\lambda^3}{k_B T} = e^{\beta\mu} + b_2 e^{2\beta\mu} + O(e^{3\beta\mu}), \quad (3)$$

where $\lambda = \sqrt{\frac{2\pi\hbar^2}{mk_B T}}$ is the thermal de Broglie wavelength, b_2 is the virial coefficient, and $e^{\beta\mu}$ is the fugacity. The virial coefficient for the Fermi gas with repulsive interaction is $b_2 = -2^{-5/2} - a/\lambda$ [30]. The pressure p was obtained from the doubly integrated density profiles [13]. The temperature was determined in the wings of the profile where $\beta\mu < -0.5$. Here, the temperature measured with and without the interaction term $-a/\lambda$ in b_2 differ by about 3%. This suggests that higher-order corrections from the interaction term will be negligible. Note that the virial expansion up to second order is valid to within 1% for the ideal gas at the density of the fitted wings.

The low-temperature normalized isothermal compressibility of a noninteracting Fermi gas is given by the Sommerfeld

expansion [31]

$$\tilde{\kappa}_{0,T} = 1 - \frac{\pi^2}{12} \left(\frac{T}{T_F} \right)^2 + O \left[\left(\frac{T}{T_F} \right)^4 \right], \quad (4)$$

where T is the temperature and T_F is the Fermi temperature. To add the effects of interactions, it is useful to work with the inverse normalized compressibility

$$\frac{1}{\tilde{\kappa}} = \frac{3}{2} \frac{2m}{\hbar^2 (6\pi^2)^{2/3}} n^{1/3} \frac{\partial \mu(n, T, a)}{\partial n}. \quad (5)$$

This is a derivative of the chemical potential, which has the following expansion in temperature and scattering length:

$$\begin{aligned} \mu(n, T, a) = E_F & \left[1 - \frac{\pi^2}{12} \left(\frac{T}{T_F} \right)^2 + \frac{4}{3\pi} k_F a \right. \\ & \left. + \frac{4(11 - 2 \ln 2)}{15\pi^2} (k_F a)^2 \right] + C T^2 a^2, \end{aligned} \quad (6)$$

where C is a constant, independent of density [32]. Therefore the inverse normalized compressibility has additive correction terms for temperature and interactions up to the second order of the interaction effect,

$$\frac{1}{\tilde{\kappa}} = \frac{1}{\tilde{\kappa}_{0,T}} + Y(k_F a). \quad (7)$$

This equation defines $Y(k_F a)$, the interaction correction to the inverse compressibility. This term is the derivative of the interaction term of the chemical potential. In second-order perturbation theory, one obtains $Y(k_F a) = \frac{2}{\pi} k_F a + \frac{8(11-2\ln 2)}{15\pi^2} (k_F a)^2$.

Figure 3 shows the normalized compressibility, the temperature T/T_F , and the interaction correction to the inverse compressibility. The temperature increases with $k_F a$ due to the increase in three-body recombination where the binding energy of the molecules ($\hbar^2/m a^2$) is transferred to the remaining atoms. The measured temperature is higher than that in previous experiments on the repulsive side [20,21]. This difference can be explained by a smaller $k_F a$ since the increase in T/T_F is approximately proportional to $1/k_F a$ [21].

We perform a linear fit of the interaction effect $Y(k_F a)$ versus $k_F a$ (constrained to pass through the origin) and obtain 0.680 ± 0.147 for the slope, in agreement with the perturbative prediction of $\frac{2}{\pi} = 0.637$. Thus we have observed the mean-field term for repulsively interacting fermions in a thermodynamic quantity. The repulsive interaction has been seen as line shifts in rf spectroscopy experiments (which, in contrast to many thermodynamic quantities, are measured independently of the kinetic energy of the atoms) [33,34]. In principle, it is possible to obtain the mean-field term directly by fitting the density profiles with an extra mean-field term. In such fits, we obtained clear evidence for such a term, but with low accuracy. It appears that the averaging over profiles for determining the compressibility (as in Fig. 2) is superior. Figure 3(c) shows the predicted effect of the second-order term on $Y(k_F a)$. With some improvements in signal-to-noise ratio, one should be able to observe this term, which is analogous to the Lee-Huang-Yang correction for bosons.

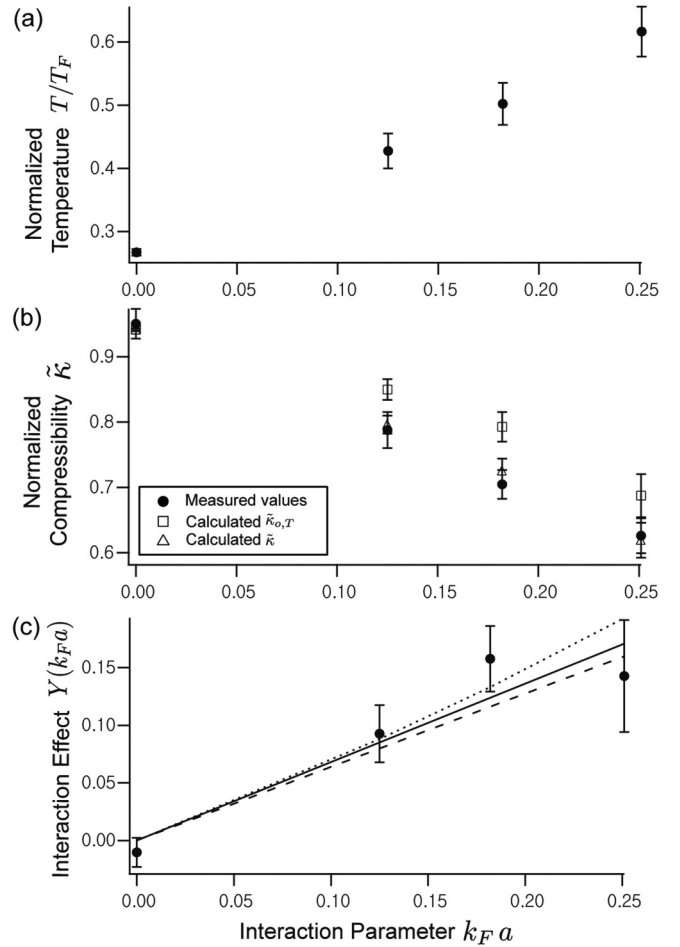


FIG. 3. Measured temperature, normalized compressibility, and interaction effect on compressibility at various interaction strengths. (a) The measured temperature as a function of interaction strength. (b) Solid circles show the measured normalized compressibility ($\tilde{\kappa}$) and open squares show the calculated normalized compressibility at the measured temperature without interaction ($\tilde{\kappa}_{0,T}$). The difference between the two indicates the effect of interaction. Open triangles show the calculated normalized compressibility using the second-order perturbation theory, which is consistent with our measured $\tilde{\kappa}$. (c) The measured interaction correction to the inverse compressibility (solid circle) is compared to a linear fit (solid line), and the first- (dashed line) and the second- (dotted line) order perturbative results.

V. DISPERSIVE EFFECT IN PHASE-CONTRAST IMAGING

As mentioned in the Introduction, phase-contrast imaging has several advantages over resonant absorption imaging, and it has been applied to many studies of cold Bose and Fermi gases [26,35,36]. Absorption imaging is usually done with absorptively dilute clouds, typically with 10% to 70% absorption (or optical densities below 1). The standard assumption has been that dispersive imaging is quantitative when the phase shift ϕ across the cloud is less than $\pi/4$. The normalized phase-contrast signal (for negligible absorption) is $3 - 2\sqrt{2} \cos(\phi \pm \pi/4)$, which is equal to $1 \pm 2\phi$ for small phase shifts [23]. The sign depends on the laser detuning and the sign of the phase shift imparted by the phase plate.

Here, we applied phase-contrast imaging for rather precise quantitative studies of ultracold Fermi gases and found that

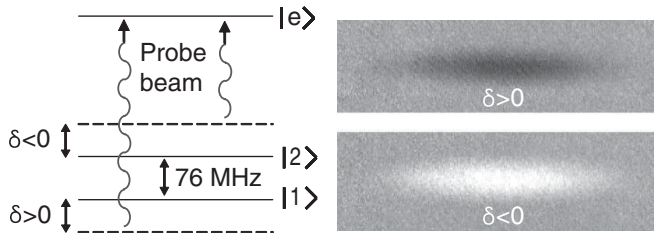


FIG. 4. Phase-contrast imaging of a balanced spin mixture in states $|1\rangle$ and $|2\rangle$. White images (phase shift $\phi > 0$) were obtained for a probe beam red detuned from the $|2\rangle \rightarrow |e\rangle$ transition, corresponding to $\delta < 0$. Black images ($\phi < 0$) were obtained for a probe beam blue detuned from the $|1\rangle \rightarrow |e\rangle$ transition, corresponding to $\delta < 0$.

even for small phase shifts systematic dispersive distortions of the image cannot be neglected. Phase-contrast imaging relies on column-density-dependent phase shifts. However, if the object is not thin, but extended along the line of sight, some lensing will affect the images. These distortions should vary in inverse proportion to the probe light detuning and become negligible for far detuning.

We investigated positive and negative detunings (δ) of 40, 80, and 120 MHz (see Fig. 4). The normalized phase-contrast image had a maximum signal of 0.35 (1.85), 0.55 (1.6), and 0.7 (1.4) for the three positive (negative) detunings. The lensing effect is opposite (focusing vs defocusing) for positive and negative detuning, and can therefore be identified by comparing profiles obtained with positive and negative detunings. Figure 5 shows that at 40 MHz, the two profiles have a visible difference, but for profiles at 80 and 120 MHz, the differences are smaller than the noise level.

However, the compressibility is determined by the slope of the profiles and very sensitive to small distortions even if they are not perceptible in the profiles. Figure 5(c) shows that, even at 120 MHz detuning, the compressibilities obtained from profiles with the two signs of the detuning differ by about 10%. Since further detuning would have resulted in a smaller signal, we evaluated the average value of the compressibility for positive and negative detuning. When the dispersive distortions are small, the effect on the compressibility should be a first-order effect in the phase shift and cancel for the average. Indeed, the average value stays constant above 80 MHz detuning. Our conclusion is that for reasonable signal levels (i.e., 50% of the baseline set by the probe light) dispersive effects are relevant for quantitative studies, but can be eliminated by performing averages over positive and negative detunings.

VI. DISCUSSION

We address now to what extent a small molecular fraction contributes to the observed density profiles. The presence of molecules is unavoidable since they form during the ramping and equilibration time. At the highest magnetic field used in the experiment, 679 G, the molecular fraction was determined to be $\sim 10\%$ (Fig. 1). The authors of Ref. [37] reported that molecules at 650 G showed an absorption cross section of about half the value of that of the atoms for probe light at the atomic resonance. For phase-contrast imaging with large detuning, molecules and atoms should contribute equally to the signal.

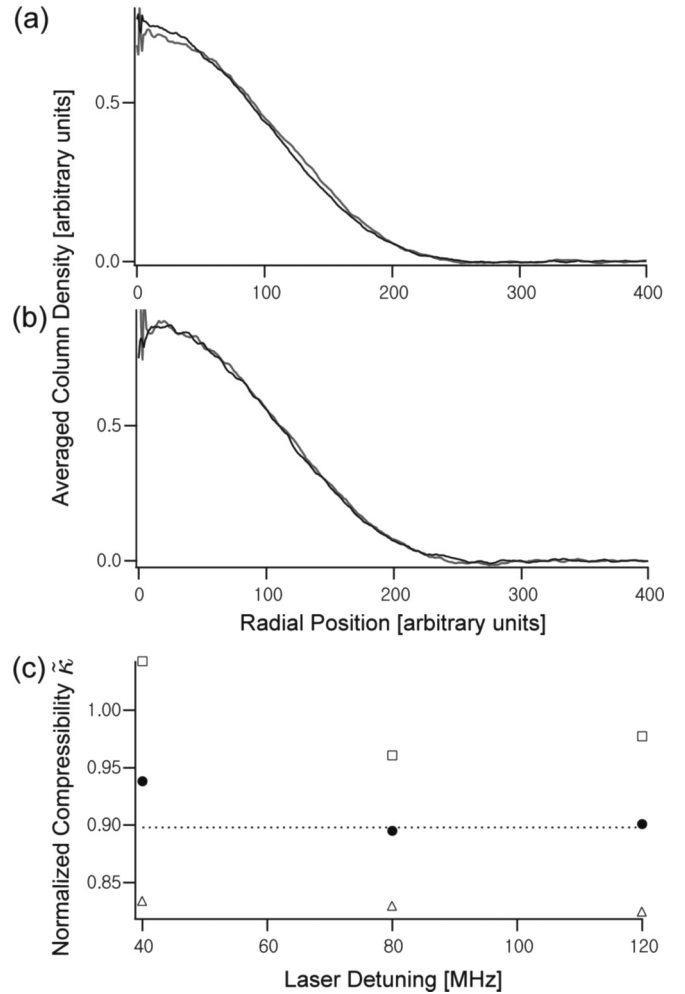


FIG. 5. Comparison of column density profiles obtained from positive and negative detunings of (a) 40 and (b) 80 MHz, respectively. (c) The measured compressibility (at $k_{Fa} = 0$) from positive- (open triangle) and negative- (open square) detuned profiles and their averages (solid circle) are shown. The average value stays constant above 80 MHz detuning.

We performed simulations to address how the presence of molecules would affect the compressibility measurements. We considered as possible scenarios (i) that the molecular fraction is constant throughout the cloud, (ii) that the molecular fraction is proportional to the loss rate ($n^{8/3}$), and (iii) that the molecular fraction is well equilibrated at the same temperature as atoms. The atomic profile is then the difference of the measured density profile and the simulated molecular density distribution. Scenario (iii) is ruled out since it would result in a rather sharp peak in the density profile, which was not observed. The first two scenarios with a 10% molecular fraction resulted in a value for the normalized compressibility which was increased by 3.3% and 4.4%, respectively. This shows that for our largest value of k_{Fa} the presence of molecules starts to become a systematic effect. In addition to the contribution to the density profiles, molecules can affect the atomic density distribution through atom-molecule interactions.

Our work shows that the interaction effect on the compressibility at the maximum possible values of $k_F a$ is about 15%. We could identify this effect only by careful thermometry (to distinguish it from thermal effects) and by correcting small dispersive distortions of the cloud. It is desirable to study fermions for stronger repulsive interactions where stronger and nonperturbative effects are predicted. The maximum possible $k_F a$ value for obtaining equilibrium density profiles is determined by the loss rate, which is proportional to $n^2 a^6 \max(T, T_F) = (k_F a)^6 n^{2/3}$ [38,39]. Therefore, the maximum possible $k_F a$ for a given loss rate is proportional to $n^{-1/9}$ and stronger interaction effects can be seen at lower density. This should be accomplished by reducing the radial confinement and not the axial confinement which determines the equilibration time. However, the weak density dependence will allow only modest increases in $k_F a$. A recent experiment used a density ten times smaller than ours [21] and reported ramping from $k_F^0 a = 0$ to $k_F^0 a = 0.35$ in 500 ms, losing only 5% of the atoms. Assuming the loss happened during the last 50 ms, we can roughly estimate a loss rate of $\sim 0.001 \text{ ms}^{-1}$ at $k_F^0 a = 0.3$, which is lower than our measurement, consistent with the lower density.

Longer lifetimes for a given $k_F a$ should be realized using narrow instead of broad Feshbach resonances. For narrow Feshbach resonances the low-lying molecular state has a dominant closed-channel character. Therefore, three-body recombination of atoms (which are in the open channel) has a smaller overlap to the molecular state and therefore a reduced loss rate. Recent experiments using rf spectroscopy [40,41] confirm this. However, for such narrow resonances the zero-range approximation is no longer valid; the interaction is no longer described by the scattering length alone and becomes

(through an effective range parameter) momentum dependent. As a result, the narrow Feshbach resonances realize a different Hamiltonian.

In conclusion, in this paper we have addressed the question to what extent Fermi gases with strong interactions can be studied by observing equilibrium density profiles. The range of sufficiently long metastability to reach equilibrium is limited to values of $k_F a < 0.25$. In this range, interaction effects are comparable to thermal effects, but we were able to observe how interactions reduce the compressibility and obtained quantitative agreement with the first-order mean-field term. An observation of the second-order Lee-Huang-Yang correction is within experimental reach.

If experiments can be performed at stronger interactions, a natural extension of our work would be a measurement of the spin susceptibility using population-imbalanced Fermi systems. This was performed recently for fermions with attractive interactions [15]. Such measurements could address the possible existence of a ferromagnetic transition in a repulsive Fermi gas [20] for which the spin susceptibility would diverge at the phase transition [42].

ACKNOWLEDGMENTS

This work was supported by the NSF and ONR, an AFOSR MURI grant, and by ARO Grant No. W911NF-07-1-0493 with funds from the DARPA Optical Lattice Emulator program. Y.-R.L. acknowledges support from the Samsung Scholarship. T.T.W. acknowledges support from NSERC. We are thankful to David E. Pritchard, Christophe Salomon, Christian Sanner, Ariel Sommer, Mark Ku, and Martin Zwierlein for valuable discussions, and Gregory Lau for experimental assistance.

-
- [1] W. Ketterle and M. W. Zwierlein, in *Ultracold Fermi Gases*, Proceedings of the International School of Physics Enrico Fermi, Course CLXIV, edited by M. Inguscio, W. Ketterle, and C. Salomon (IOS Press, Amsterdam, 2008).
- [2] Y. I. Shin, A. Schirotzek, C. H. Schunck, and W. Ketterle, *Phys. Rev. Lett.* **101**, 070404 (2008).
- [3] N. Navon, S. Piatecki, K. Günter, B. Rem, T. C. Nguyen, F. Chevy, W. Krauth, and C. Salomon, *Phys. Rev. Lett.* **107**, 135301 (2011).
- [4] N. Navon, S. Nascimbene, F. Chevy, and C. Salomon, *Science* **328**, 729 (2010).
- [5] M. J. H. Ku, A. T. Sommer, L. W. Cheuk, and M. W. Zwierlein, *Science* **335**, 563 (2012).
- [6] M. W. Zwierlein, A. Schirotzek, C. H. Schunck, and W. Ketterle, *Science* **311**, 492 (2006).
- [7] G. B. Partridge, W. Li, R. I. Kamar, Y.-A. Liao, and R. G. Hulet, *Science* **311**, 503 (2006).
- [8] M. Greiner, O. Mandel, T. Esslinger, T. W. Hänsch, and I. Bloch, *Nature (London)* **415**, 39 (2002).
- [9] I. Bloch, J. Dalibard, and W. Zwerger, *Rev. Mod. Phys.* **80**, 885 (2008).
- [10] F. Chevy, *Phys. Rev. A* **74**, 063628 (2006).
- [11] A. Bulgac and M. M. Forbes, *Phys. Rev. A* **75**, 031605 (2007).
- [12] Y. I. Shin, *Phys. Rev. A* **77**, 041603 (2008).
- [13] T.-L. Ho and Q. Zhou, *Nat. Phys.* **6**, 131 (2009).
- [14] S. Nascimbene, N. Navon, K. Jiang, F. Chevy, and C. Salomon, *Nature (London)* **463**, 1057 (2010).
- [15] S. Nascimbene, N. Navon, S. Pilati, F. Chevy, S. Giorgini, A. Georges, and C. Salomon, *Phys. Rev. Lett.* **106**, 215303 (2011).
- [16] M. Horikoshi, S. Nakajima, M. Ueda, and T. Mukaiyama, *Science* **327**, 442 (2010).
- [17] D. S. Petrov, C. Salomon, and G. V. Shlyapnikov, *Phys. Rev. Lett.* **93**, 090404 (2004).
- [18] R. A. Duine and A. H. MacDonald, *Phys. Rev. Lett.* **95**, 230403 (2005).
- [19] E. Stoner, *Philos. Mag.* **15**, 1018 (1933).
- [20] G.-B. Jo, Y.-R. Lee, J.-H. Choi, C. A. Christensen, T. H. Kim, J. H. Thywissen, D. E. Pritchard, and W. Ketterle, *Science* **325**, 1521 (2009).
- [21] C. Sanner, E. J. Su, W. Huang, A. Keshet, J. Gillen, and W. Ketterle, *arXiv:1108.2017* [Phys. Rev. Lett. (to be published)].
- [22] D. Pekker, M. Babadi, R. Sensarma, N. Zinner, L. Pollet, M. W. Zwierlein, and E. Demler, *Phys. Rev. Lett.* **106**, 050402 (2011).

- [23] W. Ketterle, D. Durfee, and D. Stamper-Kurn, in *Bose-Einstein Condensation in Atomic Gases*, Proceedings of the International School of Physics Enrico Fermi, Course CXL, edited by M. Inguscio, S. Stringari, and C. E. Wieman (IOS Press, Amsterdam, 1999).
- [24] Z. Hadzibabic, S. Gupta, C. A. Stan, C. H. Schunck, M. W. Zwierlein, K. Dieckmann, and W. Ketterle, *Phys. Rev. Lett.* **91**, 160401 (2003).
- [25] M. W. Zwierlein, C. A. Stan, C. H. Schunck, S. M. F. Raupach, S. Gupta, Z. Hadzibabic, and W. Ketterle, *Phys. Rev. Lett.* **91**, 250401 (2003).
- [26] Y. Shin, M. W. Zwierlein, C. H. Schunck, A. Schirotzek, and W. Ketterle, *Phys. Rev. Lett.* **97**, 030401 (2006).
- [27] Y. Shin, C. H. Schunck, A. Schirotzek, and W. Ketterle, *Nature (London)* **451**, 689 (2008).
- [28] A. Sommer, M. Ku, G. Roati, and M. W. Zwierlein, *Nature (London)* **472**, 201 (2011).
- [29] M. W. Zwierlein, C. H. Schunck, A. Schirotzek, and W. Ketterle, *Nature (London)* **442**, 54 (2006).
- [30] T. D. Lee and C. N. Yang, *Phys. Rev.* **116**, 25 (1959).
- [31] A. Sommerfeld, *Z. Phys.* **47**, 43 (1928).
- [32] R. K. Pathria and M. P. Kawatra, *Prog. Theor. Phys.* **27**, 638 (1962).
- [33] S. Gupta, Z. Hadzibabic, M. W. Zwierlein, C. A. Stan, K. Dieckmann, C. H. Schunck, E. G. M. van Kempen, B. J. Verhaar, and W. Ketterle, *Science* **300**, 1723 (2003).
- [34] C. A. Regal and D. S. Jin, *Phys. Rev. Lett.* **90**, 230404 (2003).
- [35] M. R. Andrews, C. G. Townsend, H.-J. Miesner, D. S. Durfee, D. M. Kurn, and W. Ketterle, *Science* **275**, 637 (1997).
- [36] D. M. Stamper-Kurn, H.-J. Miesner, S. Inouye, M. R. Andrews, and W. Ketterle, *Phys. Rev. Lett.* **81**, 500 (1998).
- [37] M. Bartenstein, A. Altmeyer, S. Riedl, S. Jochim, C. Chin, J. H. Denschlag, and R. Grimm, *Phys. Rev. Lett.* **92**, 120401 (2004).
- [38] D. S. Petrov, *Phys. Rev. A* **67**, 010703 (2003).
- [39] J. P. D’Incao and B. D. Esry, *Phys. Rev. Lett.* **94**, 213201 (2005).
- [40] C. Kohstall, M. Zaccanti, M. Jag, A. Trenkwalder, P. Massignan, G. M. Bruun, F. Schreck, and R. Grimm, *arXiv:1112.0020*.
- [41] E. L. Hazlett, Y. Zhang, R. W. Stites, and K. M. O’Hara, *Phys. Rev. Lett.* **108**, 045304 (2012).
- [42] A. Recati and S. Stringari, *Phys. Rev. Lett.* **106**, 080402 (2011).